Journal of Applied Pharmaceutical Research
Volume 13 Issue 4, Year of Publication 2025, Page 279 – 297
DOI: https://doi.org/10.69857/joapr.v13i4.1234

Check for updates

Research Article

JOURNAL OF APPLIED PHARMACEUTICAL RESEARCH | JOAPR
www.japtronline.com *ISSN: 2348 – 0335*

DEVELOPMENT OF ABEMACICLIB-ENCAPSULATED NANOSPONGES FOR BREAST CANCER: OPTIMIZATION, DRUG RELEASE KINETICS, AND IN VITRO EFFICACY

Nirosha Bolledla, Vasudha Bakshi*

Article Information
Received: 22nd April 2025
Revised: 13th July 2025
Accepted: 3rd August 2025
Published: 31st August 2025

Keywords
Abemaciclib, nanoparticle, nanosponges, breast cancer, emulsion-solvent diffusion.

ABSTRACT
Background: Abemaciclib (ABC) is a new, orally administered pharmaceutical agent authorised for the purpose of combating breast cancer. The drug's low bioavailability necessitates dosing two to three times daily, which may reduce patient compliance. To lessen the severity of side effects and prolong the duration of action, sustained-release formulations are required. Developing an ABC sustained-release nanoparticle system was the primary goal of this study. **Methodology:** Both the sustained-release polymer (EC) and the surfactant (KP-188) were derived from ethyl cellulose, in an emulsion-solvent diffusion synthesis of nanosponges (NS). We examined the impact of varying surfactant concentrations and drug-to-polymer ratios on PS, PDI, ZP, %EE, %DL, particle size, drug loading, zeta potential, and polydispersity index. **Results and Discussion:** The optimized formulation (F11) achieved an entrapment efficiency of 86.52±0.25% and a cumulative drug release of 77.12% over 24 hours. The drug release followed a sustained pattern over 24 hours. It best fits the Higuchi kinetic model, which indicates that drug diffusion was the primary mechanism of release from the matrix system. The MTT experiment demonstrated that ABC might be a viable cytotoxic nanocarrier for breast cancer cells from humans, specifically MCF-7 and MDA-MB-231. On top of that, following contact with storage settings of 25, 5, and 45 °C for six months, ABC maintained its drug release property with no modification in the percentage release. **Conclusion:** This study shows that the created NS could effectively transport and release ABC, amplifying its impact in the battle against breast cancer.

INTRODUCTION

There have been around 2.6 million female cancer diagnoses and approximately 685,000 fatalities worldwide due to breast cancer (BC), resulting in it being a top cause of death from cancer [1]. BC has emerged as the main factor in the mortality of around 30% of individuals with cancer across all kinds [2]. In 2021, more than 30% of all female malignancies will be breast cancer, making it one of the top four malignancies in women [3]. Death rates have dropped dramatically with combined chemotherapeutic methods, particularly in early-stage female

*Department of Pharmaceutics, School of Pharmacy, Anurag University, Venkatapur, Ghatkesar, Medchal-Malkajgiri, Hyderabad – 500 088, Telangana, India.

***For Correspondence:** **vasudhapharmacy@anurag.edu.in**

diagnoses, as compared to mono-therapy [4]. Acquired pharmacological resistance increases the likelihood of recurrence [5]. A lot of people are thinking about & interested in targeted chemotherapeutics since they exhibit inhibitory activity against the target location with little off-target effects [6]. Research indicates that cell-cycle development in mammalian cells is rigorously regulated by a group of cyclin proteins, which sequentially associate with and activate serine-threonine kinases known as cyclin-dependent kinases [7-8]. Additionally, it has been shown that several genetic abnormalities, including the overexpression of cyclin D1, alter the course of biological processes in breast cancer cells, which are seen in around 50–70% of patients [9-10].

Clinical studies were conducted using flavopiridol, a first-generation CDK4 and CDK6 inhibitor, and the researchers have reported on its therapeutic efficacy [11]. Its toxicity and other negative consequences were the result of its inability to target certain targets selectively [12]. While flavopiridol alone did not demonstrate much effect, it was shown to enhance apoptosis when coupled with docetaxel [13]. Subsequently, dinaciclib, a second-generation CDK inhibitor, showed improved selectivity; nevertheless, it was subsequently withdrawn from Phase I and Phase II clinical trials owing to very high levels of toxicity [11, 14-15]. The subsequent generation of CDK inhibitors outperformed their predecessors in several ways, including improved selectivity in targeting both CDK4 and CDK6, and the ease of oral administration [16-18]. To inhibit only CDK4 and CDK6, palbociclib (PD-0332991) was initially introduced in 2004 [19]. Afterwards, the CDK4 and CDK6 inhibitors LY-2835219 and ribociclib (LEE011) were created [20-21]; other forms of cancer, such as non-small-cell lung, breast, colon, etc., have been studied in clinical trials. Its uses in breast cancer therapy have also been heavily sanctioned by the FDA and other regulatory bodies [22-24]. Their anticancer effects are mainly because these inhibitors prevent the G1/S transition-related gene transcriptions from taking place by inhibiting cyclin D-dependent protein kinases CDK4 and CDK6. This, in turn, inhibits Rb phosphorylation [25]. A lipophilic cavity and a hydrophilic surface characterise this polymer derived from natural polysaccharides. There are limited uses for natural cyclodextrin because its lipoidal core cannot accept hydrophilic and large-sized moieties [26]. In addition, cyclodextrins are poorly soluble in water due to the strong intermolecular hydrogen bonds that exist in their crystal form [27]. The formation of cyclodextrin nanosponge (CDNS) is achieved by a small-scale chemical alteration of native cyclodextrin through a reaction with a cross-linker [28]. The nanochannels of sponges and the cavities of natural cyclodextrins may accommodate both hydrophilic and lipophilic molecules [29]. Nanosponge based on cyclodextrin is typically synthesised using one of four methods: the melt technique, solvent evaporation, ultrasound-aided synthesis, or microwave-assisted synthesis [30]. In Nanosponges formulations, cyclodextrin is used to increase the solubility and stability [31] and increases the bioavailability of poorly water-soluble drugs [32]. Abemaciclib pharmacokinetic limitations, including its low aqueous solubility, limited oral bioavailability, and dose-limiting gastrointestinal toxicity, present challenges for conventional delivery systems [33]. Conventional nanoparticulate systems such as solid lipid nanoparticles (SLNs), nanostructured lipid carriers (NLCs), and liposomes have shown promise in improving drug solubility and targeting. However, these systems often face challenges like low drug loading, physical instability, and burst drug release. In contrast, cyclodextrin-based nanosponges offer a robust and porous structure that allows higher entrapment efficiency, sustained release, and greater stability, making them particularly suitable for the delivery of hydrophobic drugs like Abemaciclib. "Nanosponges" (NS) are small, self-explanatory, three-dimensional structures that resemble a mesh and have a size less than 1 µm [32]. Various medicines, proteins, peptides, nucleic acids, oils, and gaseous substances may form complexes with these nanocarriers, either inclusion or non-inclusion [33].

Research on nanosponge formulations has shown promising results in cancer treatment, with improved efficacy in both laboratory and preclinical investigations. Not only that, these delivery methods are harmless when taken orally, biocompatible, and biodegradable. To enhance the encapsulation of the visiting medication, hydrophilic polymers are added to the nanosponge system. Accordingly, this work set out to improve the effectiveness of existing breast cancer treatments by creating ABC-loaded ternary NS and then evaluating them physicochemically, *in vitro*, and cytotoxically against MCF7 and MDA-MB-231 human breast cancer cells.

MATERIAL AND METHOD

Materials

Eli Lilly Pvt Ltd. of Gurugram, Haryana, was the source of the Abemaciclib (ABC) ≥ 99% purity that was bought. " Sigma Aldrich International, Inc., India Dulbecco's Modified Eagle's

Medium (DMEM), dimethyl sulfoxide (DMSO), dichloromethane (DCM), and foetal bovine serum (FBS) were all sourced from here. Every other chemical and solvent was used exactly as it was supplied.

Preparation of nanosponges

A process called solvent emulsification-ultrasonication was used to manufacture ABC-encapsulated NS, or ABC-NS for short. A variety of NS with different compositions were created by using different quantities of β-cyclodextrin (β-CD), crosslinker, and DMF. Dilute 50 mg of ABC (i.e., drug) in 1 mL of N, N-methylene bisacrylamide and 4 mL of γ-CD in DCM was used to dissolve the drug and polymer entirely. An IKA® VORTEX 3 vortex shaker, manufactured in Staufen, Germany, was used to vortex both solutions independently. The mixture was thoroughly mixed using probe sonication "(probe # 423, CL-18, Fisher Scientific; USA)" working at 65% W for 5 minutes with a 10-second pulse on-off cycle after the organic phase was added dropwise to the water phase containing the crosslinker. The beaker containing the drug-loaded dispersion solution was subjected to magnetic stirring at 700 rpm following the evaporation of the organic solvent. The adsorbed drug and free-dried "(Martin Christ Alpha-1-4LD freeze-drier, Osterode, Germany)" particles were rinsed off with Milli-Q water (n = 3) after centrifuging the concentrated dispersion at 11,000 rpm for 15 minutes [34].

Factorial design for formulation of ABC-NS

We began by conducting trial experiments to identify the most crucial variables and to determine the optimal values. The EE, zeta potential, and size of the vesicles were investigated in relation to the three variables: surfactant speed, polymer concentration, and agitation speed. Cyclodextrin crosslinker and DMF concentrations, ranging from 25 to 150 mg, 50 to 125 mg, and 5 to 20 mL, were identified as the most significant factors after preliminary screening. A three-level Box-Behnken design was used to analyse the relationship between the independent factors and the dependent variables, which were defined by the results of the preliminary tests: particle size (PS), entrapment efficacy (EE), polydispersity index (PDI), and zeta potential (ZP). This configuration is highly effective when constructing models of second-order polynomials and examining quadratic response surfaces. The design comprises numerous repetitions of the same central points, in addition to a collection of midpoints along each cube's edge that defines the three-dimensional area of focus. The experimental domain variables' response surfaces were examined using Stat-Ease design expert software. Following that, the experimental statistical method was validated once more through three additional confirmation investigations. A quadratic equation was derived from seventeen experimental iterations in response to the three-factor, three-level design, which described the model as mentioned in Table 1 [35]. The following equation (1) illustrates this:

$$Y = b0 + b1x1 + b2x2 + b3x3 + b4x4 + b12x1x2 + b13x1x3 + b23x2x3 + b11x21 + b22x22 + b33x23 \quad \text{…….(1)}$$

Several variables, including the intercept (b0), regression coefficients (b1–b3), independent variables (x1–x3), interaction coefficients (b12, b13, b23), and quadratic coefficients (b11, b22, b33), were incorporated into the experiment. The outcome was the manifestation of an effect that occurred when different levels of process parameters were combined.

Table 1: Formulation composition constraints of ABC-NS.

Parameter	Low (-1)	Medium (0)	High (+1)
Independent Variables			
X1: Cyclodextrin (mg)	25	87.5	150
X2: Crosslinker (mg)	50	87.5	125
X3: DMF (mL)	5	12.5	20
Dependent variables	**Constrains**		
Y1: Particle size [nm]	Minimize		
Y2: %EE	Maximize		
Y3: PDI	In range		
Y4: Zeta potential	Target		

Optimization of ABC-NS

Dedicated to producing the highest quality NS, we identified the quality target product profile (QTPP). This phase was critical in ascertaining the probable attributes of the product. To guarantee that the ultimate product satisfies all criteria relating to quality, safety, and efficacy, due consideration must be devoted to this particular stage. Nevertheless, without paying special attention to CPP (certificate of pharmaceutical product) and CMA (certified medication aide), which may affect CQA (critical quality attributes), it would be impossible to accomplish this objective. Table 1 contains a list of the numerous QTPP essentials and their validation for ABC-NS production. The research must address these specific QTPP objectives. For instance, it would be optimal if the manufactured product possessed attributes that enable its application topically [36].

Characterization

The average particle diameter and ABC-NS PDI were calculated by an approach that made use of dynamic light scattering, a technique developed by Malvern Instruments in the United Kingdom (Zetasizer Nano ZS instrument). To break up particle agglomerates, the samples to be studied were diluted with Milli-Q water (1:200) and then subjected to sonication for 2 minutes. After that, the cuvette that had been attached to the electrode made of copper alloy was filled with diluted particle dispersion. The particle analyser was thereafter loaded with the sample holder. The settings were adjusted to analyse particle size & potential as the laser beam passed at 900. A total of three separate measurements were made for each parameter. A Zetasizer Nano ZS device, made in the UK by Malvern Instruments, was used to find the ZP value of each nanosponge. Diluting samples before transferring them to a glass electrode was the only variation in the ZP measurement process [37]. The drug loading (DL) and entrapment efficacy (EE) in each formulation's nanosponges were determined using an indirect technique. A 10-minute centrifugation run at 12,000 rpm was performed on the newly made nanosponge solution (Hermle Labortechnik, Z216MK, Wehingen, Germany). When measuring UV-spectrophotometry, a Japanese company called Jasco utilised a V-630 model. We analysed the supernatant of each sample after centrifugation. The samples were collected in microcentrifuge tubes. The following formulae were used to determine the % EE and % DL by equations (2) and (3), respectively [37]:

$$\%\boldsymbol{EE} = \frac{\boldsymbol{Td-Sd}}{\boldsymbol{Td}}\boldsymbol{X100} \qquad \text{……. (2)}$$

$$\%\boldsymbol{DL} = \frac{\boldsymbol{Total\ entraped\ drug}}{\boldsymbol{weight\ of\ nanosponge}}\boldsymbol{X100} \text{ …….. (3)}$$

Fourier-transform infrared (FTIR) analysis

The purpose of the FTIR analysis was to determine whether the stabilisers and polymers used to construct the nanosponges were compatible with ABC. An FTIR spectrometer from Tokyo, Japan, the Jasco 4600 Mid-IR, was used to determine the fingerprint area of the ABC in optimised NS by mixing potassium bromide (KBr) with both ABC and optimised NS separately, then compressing the mixture into a disc and scanning it from 4000 to 400 cm^{-1}. One of the dependable, practical & cost-effective methods for FTIR is a qualitative research tool. The materials' characteristics & interactions are quickly revealed by the positioning and strength of the peaks [38].

Differential scanning calorimetry (DSC) analysis

An optimal NS was performed with a hemispherical aluminium pan and a heating rate of 20 °C/min. Scinco of Seoul, Korea, manufactured a DSC N-650, and it was used to perform the physicochemical drug-excipient interaction for ABC. Testing included the passage of nitrogen gas, and software was used to process and composite the temperature peaks of the samples for interpretation [39].

X-ray diffraction (XRD)

The crystal structure/ crystallography of the materials was studied by characterising optimised NS using XRD analysis on samples. Once the substance was placed on a sample holder, the intensity and angle of the scattered X-rays were measured using ionised radiation (X-rays) within a 2θ range of 5-75 °C. By analysing and interpreting the XRD diffraction pattern, the physical state parameters and crystal structure of the material might be determined. Tokyo, Japan's Siemens D5000 Diffractometer generates diffractogram data that reveal the atomic and molecular lattice-based crystallinity and molecule adduct type [40].

Scanning electron microscopy (SEM)

To prevent damaging the sample, optimised NS were subjected to an electron beam under negative pressure with an acceleration voltage of 5 kV and a beam current of 20 mA (SEM-Ultraplus, Jena, Germany). After the substrate was thinned and the sample was attached using conductive glue, an enhancement in the sample's electron conductivity was achieved by coating it with gold. After making both large-scale and detailed adjustments visibly on the screen, the sample was scanned from the designated location, and photographs were then taken [41].

***In vitro* diffusion study**

To examine the optimised ABC-NS's drug release behaviour and kinetic mechanism, an in vitro drug diffusion study was conducted. By using the dialysis membrane (MWCO: 14kDa) technique, the diffusion of both the pure drug (ABC) and F11 was studied. In 5 mL of diffusion medium (phosphate buffer, pH 7.4), pure ABC (10 mg) and an equal quantity of NS were distributed separately. Afterwards, the ABC and ABC11 suspensions were mixed with 100 mL of pH 7.4, which was used to simulate physiological conditions, as this pH closely mimics the extracellular environment of blood and most normal tissues. This choice helps evaluate the drug release behavior under

conditions relevant to systemic circulation before being inserted onto the porous dialysis membrane tubing (MD-25-14) made of regenerated cellulose. Afterwards, the tube's two ends were connected. The assembly was placed on a magnetic stirrer that could be controlled by a thermostat, enabling a steady stirring speed of 50 rpm and a physiological temperature of 37±1 ^{0}C to be maintained. To replicate a sink scenario, two millilitres of material were periodically withdrawn and replaced with an equivalent volume of newly made diffusion media. The cumulative release profile was mapped out by examining the aliquots three times at 296 nm with a UV-Vis Spectrophotometer (JascoUV/Visible Spectrophotometer V-630, Japan). The mechanism of F11 release was determined by matching the drug release data with a range of mathematical models. Kinetic models such as Zero-order, First-order, Higuchi-Matrix, and Korsmeyer Peppas were included in this set of equations (4) to (7), respectively [42]:

$$\boldsymbol{Zero-order}: \quad \boldsymbol{Q_t = Q_0 + K_0 t} \quad \ldots\ldots (4)$$

$$\boldsymbol{First-order}: \quad \boldsymbol{logQt = logQ0 - k1t/2.303} \ldots..(5)$$

$$\boldsymbol{Higuchi}: \quad \boldsymbol{Q = K_H t^{\frac{1}{2}}} \quad \ldots\ldots\ldots (6)$$

$$\boldsymbol{Korsmeyer-Peppas}: \quad \boldsymbol{Mt/M\infty = ktn} \quad \ldots\ldots (7)$$

Given that the drug concentration at time t is denoted as Q_t and the drug concentration at the beginning of diffusion is denoted as Q_0, the rate constants for the zero-order, first-order, and Higuchi models are k_0, k_1, and $k_H t_{1/2}$, respectively. In contrast to M∞, which stands for infinite duration, Mt denotes the cumulative drug release at time t. The structural and geometric properties of I-NS are represented by the rate constant k, the release mechanism by the diffusional exponent n, and the period of release by the symbol t. Each of those models likewise displayed the correct parameters, and to assess the release kinetic behaviour of ABC, the coefficient of multiple determination, denoted as R^2 and ranging from 0 to 1, was utilised. The processes of release were also taken into account in reference. A value of n = 0.45 indicates Fickian diffusion, a value between 0.45 and 0.89 indicates aberrant behaviour or non-fickian transport, a value of n = 0.89 indicates Case II transport, and a value greater than 0.89 indicates supercase II [42].

Antioxidant Activity

The 2,2′-diphenyl-1-picryl hydrazyl test (DPPH assay) with a modest modification was used to evaluate the antioxidant activity of the improved, optimised ABC-NS to that of pure ABC and ascorbic acid, a common antioxidant. 4 mg of DPPH was added to 100 mL of methanol to create the DPPH solution (0.1 mM). I used serial dilution to create F11, pure ABC, and ascorbic acid solutions with concentrations ranging from 1 to 100 µg/mL. 2 mL of a 0.1 mM DPPH solution was mixed with 0.5 mL of methanol to make a blank mixture (control), and 0.5 mL of each concentration was added separately to make a reaction mixture. All reaction mixtures were left to incubate for 30 minutes without illumination at room temperature (25 °C). By utilising a "(V-630, JASCO International Co., Ltd., Hachioji, Tokyo, Japan)" UV-VIS spectrophotometer, the absorbance of reaction mixtures at 517 nm was determined. Antioxidant activity determined by equation (8), which is measured in percent DPPH scavenging [43].

$$\% \boldsymbol{Antioxidant\ activity} = \frac{\boldsymbol{Ab-At}}{\boldsymbol{Ab}} \boldsymbol{X100} \quad \ldots\ldots\ldots (8)$$

MTT assay

In vitro cytotoxicity experiments were performed on human breast cancer cells MCF-7 and MDA-MB-231 by means of the MTT (3-[4,5-dimethylthiazole-2-yl]2,5-diphenyltetrazolium bromide) test, with both the pure ABC suspension and F11 utilised. Initially, in a 37±1°C, 5% CO_2 environment, carcinogenic cell lines MCF7 Cells from both the MDA-MB-231 and a control group were cultured in a medium containing 10% FBS and supplemented with DMEM. After that, a 24-well plate was seeded with 1 mL of cultivated cell suspension (about 5×10^1 cells/mL) and left undisturbed in the incubator overnight. Each of the 96-well plates was pre-treated before the samples under study were inserted. In the following steps, 100 µL of a 5% w/v MTT solution was added to each well and left to incubate at 37 °C for an extra four hours [44]. A Thermo Fisher Scientific, USA-made ELISA microplate reader was also used to measure the absorbance of each sample at 490 nm. The cell viability % determined by Eq. (9):

$$\% \boldsymbol{cell\ viability} = \frac{\boldsymbol{Mean\ absorbance\ of\ test\ sample}}{\boldsymbol{Mean\ absorbance\ of\ control}} \boldsymbol{X100} \ldots.. (9)$$

Statistical Analysis

The data was statistically analysed by GraphPad Prism (version 4), a program created and owned by GraphPad Software in San Diego, CA, USA. An analysis of variance using Tukey's post hoc test and a one-way ANOVA were part of the procedures. We considered $p < 0.05$ to be the significant criterion [45].

RESULTS AND DISCUSSION

Evaluation of Abemaciclib-loaded NS

The purpose of producing seventeen ABC-NS with varying amounts of cyclodextrin, crosslinker, and DMF was to evaluate

the impact of formulation composition on characteristics (Table 2). Size distribution, PDI, ZP, and percentage of drug encapsulation were the parameters tested for in the manufactured NS. The improved formulations were then tested against breast cancer cell lines *in vitro* using the MTT assay, *in vitro* release studies, and morphology [35-45].

Table 2: Design and optimization of independent variables for ABC-NS

Std.	Run	X1	X2	X3	PS	EE	PDI	ZP
14	**1**	87.5	87.5	12.5	183.26±3.62	76.45±0.25	0.274±0.02	-15.34±1.24
2	**2**	150	50	12.5	212.36±2.51	71.54±0.36	0.298±0.01	-16.57±1.03
10	**3**	87.5	125	5	263.51±1.24	60.28±0.85	0.506±0.04	-27.41±1.26
8	**4**	150	87.5	20	202.31±3.06	73.95±0.41	0.317±0.03	-29.84±1.25
15	**5**	87.5	87.5	12.5	190.53±5.31	73.02±0.28	0.265±0.05	-17.84±0.95
11	**6**	87.5	50	20	198.67±2.48	80.94±0.37	0.331±0.06	-19.62±0.67
6	**7**	150	87.5	5	291.04±1.36	48.76±0.61	0.518±0.08	-30.26±0.85
4	**8**	150	125	12.5	263.51±1.25	57.82±0.25	0.479±0.12	-29.51±1.16
3	**9**	25	125	12.5	228.96±2.05	74.69±0.41	0.375±0.13	-14.59±1.24
9	**10**	87.5	50	5	217.94±3.42	75.34±0.39	0.352±0.02	-18.35±0.39
12	**11**	**87.5**	**125**	**20**	**155.36±2.61**	**86.52±0.25**	**0.275±0.31**	**-17.35±0.85**
7	**12**	25	87.5	20	234.75±1.58	68.25±0.81	0.446±0.15	-21.78±0.61
5	**13**	25	87.5	5	258.97±1.42	58.36±0.34	0.426±0.14	-25.84±0.49
16	**14**	87.5	87.5	12.5	192.69±3.02	78.96±0.12	0.281±0.15	-14.23±1.24
1	**15**	25	50	12.5	245.31±2.61	67.35±0.25	0.395±0.31	-21.96±1.25
13	**16**	87.5	87.5	12.5	195.26±2.48	74.98±0.62	0.269±0.16	-15.62±1.36
17	**17**	87.5	87.5	12.5	186.43±3.15	80.31±0.25	0.269±0.15	-13.56±1.24

X1 – Cyclodextrin; X2 – β-cross linker; X3 – DMF; Y1 – PS; Y2 – EE; Y3 – PDI, Y4 – ZP

Effect of independent variables on response 1 (Particle size): An impact is considered positive in this polynomial equation when the sign (+) is used, and negative when the symbol (-) is used. Answer 1's polynomial equation for particle size as a function of coded components is the size of a particle:

$$PS = +189.63 + 0.1538A + 4.63B - 30.05C + 16.87AB - 16.13AC - 22.22BC + 42.90A2 + 5.00B2 + 14.23C2 \quad \text{……..…….(10)}$$

A slight positive influence of cyclodextrin concentration on particle size. This could be due to increased viscosity of the dispersion medium, leading to larger particles due to inefficient shearing and coalescence during emulsification. B: Higher stirring speeds lead to slightly larger particles, which may seem counterintuitive, but beyond a critical shear force, turbulence may promote collision and agglomeration. C: Increasing the crosslinker volume significantly reduces particle size, likely due to more effective crosslinking and structural compaction of the nanosponge matrix. AB: At higher cyclodextrin concentrations and stirring speeds, the system may trap more solvent or form less defined structures, increasing particle size. AC, BC: These negative interactions suggest that combining higher CD or stirring speed with sufficient crosslinker helps reduce particle size, likely due to improved matrix tightening or dispersion. A^2, B^2, C^2: These positive coefficients indicate that too high a level of each variable causes a rise in particle size, likely due to oversaturation, turbulence, or crosslinking-induced aggregation. Equation (10) and Figure 1 suggest that the size of the prepared nanosponges is positively affected by the concentration of cyclodextrin (A). This is corroborated by the fact that, as desired, bigger particles were produced at greater cyclodextrin concentrations and by the statistical significance of the positive coefficient of the term A (p=0.0320). In contrast to nanosponges made with 87.5 mg of cyclodextrin, which had an average particle size of 155.36±2.61 nm, nanosponges generated with 25 mg of cyclodextrin had an average particle size of 234.75±1.58 nm. The surface tension between the continuous and scattered phases may have been reduced at larger concentrations, which might explain the observed phenomenon. A similar agonistic effect is seen for the crosslinker concentration (B), which suggests that a higher crosslinker intensity results in a smaller

particle size. Due to an increase in mechanical shear caused by a high amplitude, particle size is reduced when the surfactant intensity is high. Consequently, nanosponge particles become finer as a result of the formation of smaller emulsion globules. Whereas slower stirring speeds increase the globules' ability to combine and create larger particles. Our research also shows that increasing the concentration of the surfactant (BC) and polymer (AC) together has the desired effect, the particle size decreased, which is obviously not what we want. To achieve the desired result of smaller particles, we should maintain a high polymer concentration and a low surfactant concentration, and sonicate the mixture more vigorously.

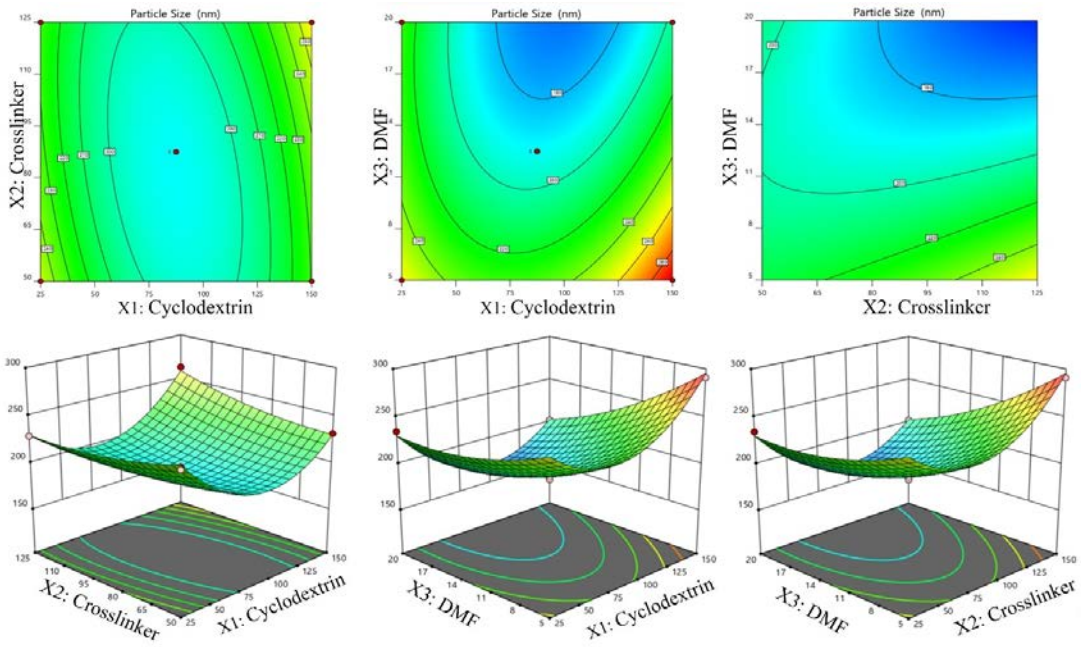

Figure 1: Effect of independent variables of particle size counter and response surface plots

The model is considered statistically significant with an F-value of 64.05. With a probability of just 0.01%, random chance is the only plausible explanation for such a high F-value. Model terms are considered statistically significant if their p-value is less than 0.0500. A^3, C^3, C, AB, AC, BC, and C^3 are the essential terms in this model. The effect is obviously minor when compared to the blatant error; the F-value for Lack of Fit is 2.29, indicating. The likelihood of noise producing the significant Lack of Fit F-value is 22.05%. With a difference of less than 0.2, the Adjusted R^2 and the Predicted R^2 are pretty close to each other, coming in at 0.9726 and 0.8718, respectively. Adequate precision is one tool for determining signal-to-noise ratio. The optimal ratio is greater than 4. The signal-to-noise ratio should be at least 28.671 for optimal performance. Navigating the design area will be a breeze with this model.

Effect of Independent variables on response 2 (entrapment efficiency)

The formed nanosponges are believed to contain the most significant quantity of medication since the proportion of ABC trapped inside them varies from 48.76±0.61 to 86.52±0.25%. Equation including coded components for answer 2-EE: Equation (EE) may be written as below, equation (11):

$$EE = +76.74 + 2.07A - 1.98B + 8.37C - 5.27AB + 3.83AC + 5.16BC - 11.17A2 + 2.27B2 - 3.25C2 \quad \text{.....(11)}$$

A: Higher CD concentration increases EE due to more cavity sites and greater matrix availability for drug entrapment. B: Higher stirring speed negatively affects EE, likely due to shear stress leading to drug leakage or unstable micro-droplets during formulation. C: More crosslinker increases EE significantly, as it stabilizes the nanosponge matrix and locks in drug molecules more effectively. AB: High CD with high speed may destabilize the emulsion, lowering EE. AC, BC: The crosslinker works synergistically with CD, thereby accelerating the enhancement of drug retention within the nanosponge. A^2: Excess CD reduces EE, possibly due to saturation or overcomplexation. B^2, C^2: Stirring speed has a minor beneficial effect at optimal levels, while excess crosslinker might compact the network too tightly, reducing drug entrapment. Figure 2 and equation (11) suggest that, with a statistically significant (p = 0.0096) negative impact, factor A (polymer concentration) reduces the electrostatic

energy (EE) of the nanosponge formulation. Reasons for this could include the following: first, the organic phase has more room to accommodate the drug owing to polymeric entanglement, which increases drug entrapment; second, the medium's viscosity increases with increasing polymer concentration; and third, the nanosponge carriers solidify faster, stopping the medication from diffusing into the formulation's water phase.

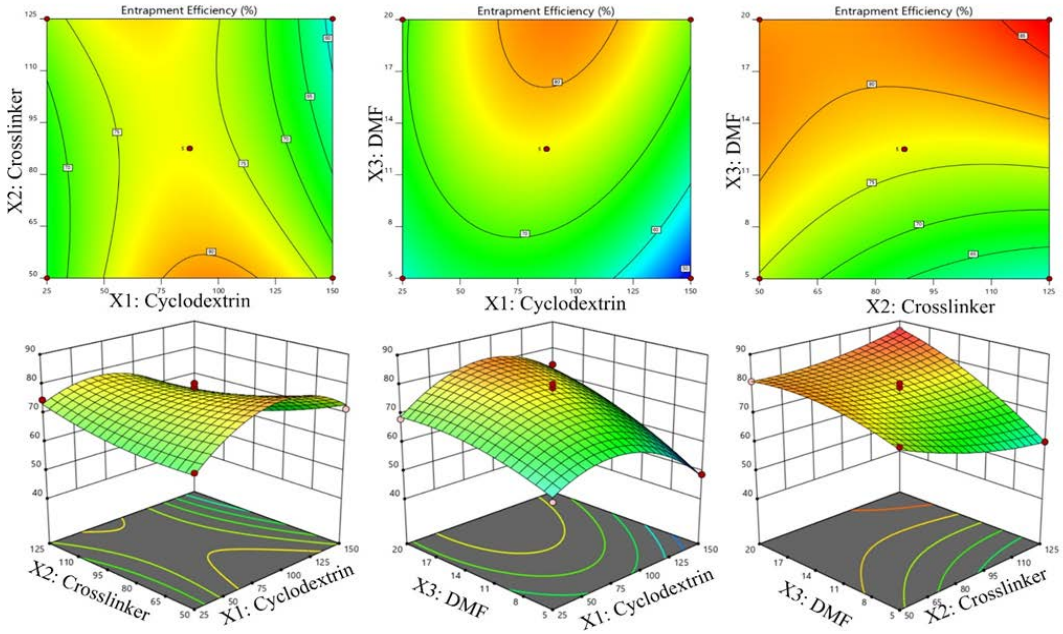

Figure 2: Contour response surface plot interaction between the independent variables on the EE

Given that the sign of the coefficient B is statistically significantly negative (p = 0.0027), the opposite impact of surfactant concentration on EE is a reduction in EE as the concentration of surfactant increases. Since the used surfactant is a larger molecule, molecular concentrations are organised at a distance from the point of oil-water contact; these molecules are not ionic. A reduction in the formulation's % EE occurs as a result of the medication dissolving in this hydrophobic area. Another probable explanation might be the solubilisation effect, which occurs when the drug is dissolved in the aqueous phase of a formulation as the concentration of surfactant increases. Therefore, increasing the surfactant concentration would result in a decrease in the quantity of medication that would be entrapped. The impact on %EE of components AB is synergistic; that is, increasing the concentration of both polymer and surfactant in the right proportions yielded the best percentage EE values. An F-value of 24.87 indicates that the model is statistically significant. The likelihood of an F-value this high being attributable to noise is less than 0.02%. The model terms are deemed significant if the p-value is below 0.0500. The following terms—C, AB, AC, BC, A^3, and C—are important in this model. With an F-value of 0.47 for Lack of Fit, the pure mistake is more important than the Lack of Fit. There is a 72.12% probability that noise is the cause of a Lack of Fit F-value of this magnitude. There is a negligible difference (less than 0.2) between the expected R^2 of 0.8391 and the modified R^2 of 0.9307. The signal-to-noise ratio can be measured with Adeq Precision. It is ideal if the ratio is higher than 4. With 19.780, you have an adequate signal-to-noise ratio. The design space can be explored with the help of this model.

Effect on PDI

The A/C interaction on EE with a constant value of C and the A/B interaction on PDI with a constant value of B. Y3 decreased from 0.274±0.02 to 0.506±0.04 at low A levels. Y3 also decreased from 0.275±0.31 to 0.331±0.06 at high A levels. Response optimisation followed the generation of polynomial equations linking dependent and independent variables (Figure 3). To achieve the intended results, the optimum values for the process variables were determined through numerical optimization using the desirability technique. We achieved optimal circumstances by imposing limits on both variables and PDI determined by following Eq. (12).

$$PDI = +0.2756 - 0.0037A + 0.0324B - 0.0541C + 0.0502AB - 0.0553AC - 0.0525BC + 0.0859A2 + 0.0252A2 + 0.0652C2 \quad \text{.....(12)}$$

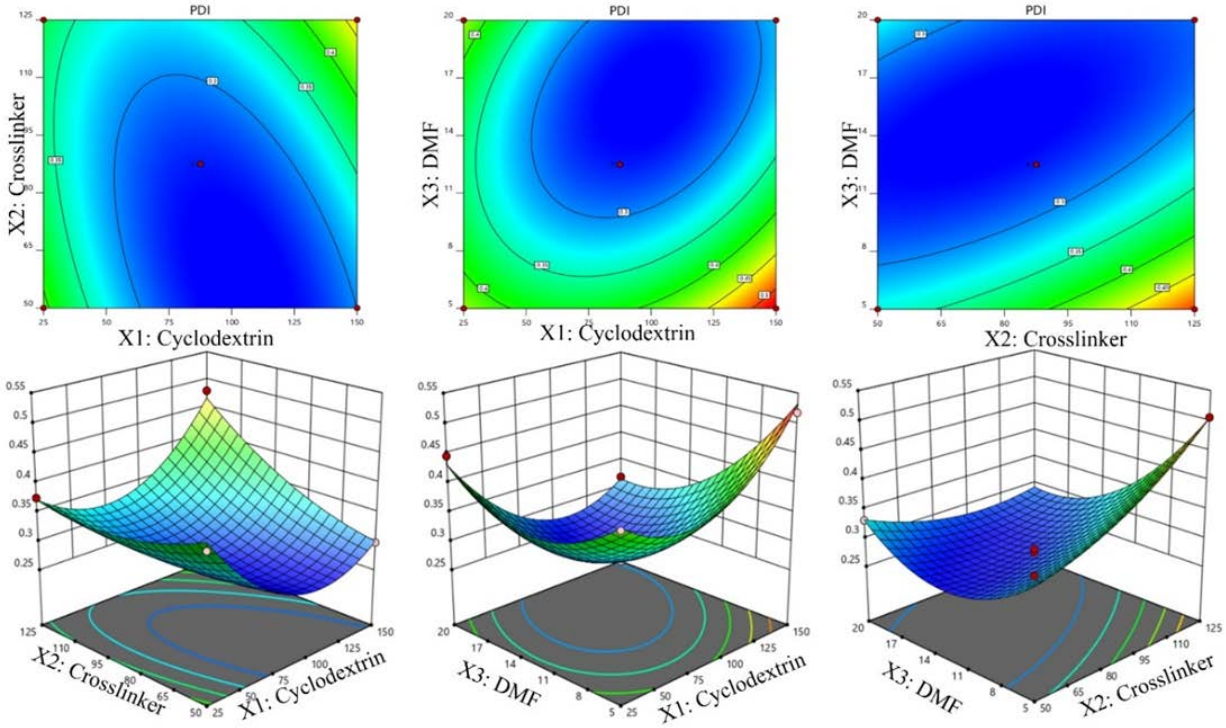

Figure 3: Contour response surface plot interaction between the independent variables on the PDI

A: Cyclodextrin has a negligible influence on PDI alone, showing a neutral effect on homogeneity. B: Stirring speed increases PDI slightly, suggesting greater size variability at higher speeds. C: Cross-linker reduces PDI, indicating that it helps produce more uniform particles. AB: Higher CD and speed increase size variability (broader distribution). AC, BC: Combined effects with crosslinker reduce PDI, enhancing uniformity. All positive, meaning extremes in variable values increase polydispersity due to instability or secondary particle growth. The statistical significance of the model is demonstrated by an F-value of 64.01. Such a high F-value could only have been a coincidence, given the extremely low probability of its occurrence (0.01%).

The model terms are considered significant when the p-value is less than 0.0500. In this scenario, major model variables include B, C, AB, AC, BC, A^2, B^2, and C^2. The model terms are not considered significant when the values are more than 0.1000. There is a notable Lack of Fit if the F-value is 12.07. There is a 1.79 percent chance that noise will produce an F-value this high. The expected R^2 of 0.8252 and the modified R^2 of 0.9726 are nearly identical; the difference is less than 0.2. You can use Adeq Precision to measure the signal-to-noise ratio. It is ideal if the ratio is more than 4. An excellent signal-to-noise ratio of 23.128 indicates successful outcomes.

Effect of independent variables on zeta potential

The positive values of the two independent variables in the equation suggest that the ABC-NS formulations have a restricted zeta potential. The zeta potential is a totally autonomous response to X1–X3, and their interplay is evident from this. Further evidence that the zeta potential was a phenomenon that depended on particle size is provided by this. In Figure 4, the ZP ranges from -13.56 ± 1.24 to -30.26 ± 0.85, with the predicted values for cyclodextrin and PVA combinations being -1 and +1, respectively. For a deterministic test of independent variables, the whole factorial design's zeta potential (Y4) is presented in Table 2.

The optimised NS zeta potential was -24.36±3.26, indicating that the zeta potential was unaffected by the amounts of cyclodextrin and PVA used in the investigation, as the experimental values exceeded the equation's anticipated value for all ABC-NS formulations.

$$\boldsymbol{ZP = -15.32 - 2.45A - 1.55B + 1.66C - 5.08AB - 0.9100AC + 2.83BC - 5.79A2 + 0.4540B2 - 5.82C2} \quad \text{……..…….(13)}$$

A, B: Increasing cyclodextrin and speed reduces zeta potential (more negative), likely due to more exposure of surface charges or ionic species. C: More cross-linker slightly reduces the magnitude of surface charge, likely due to shielding of surface functional groups. AB: High CD and speed synergistically decrease ZP (more negative), improving electrostatic repulsion and potentially stability. BC: Stirring and cross-linking together slightly increases surface neutrality. A^2, C^2: Extremes in CD and cross-linker sharply reduce ZP (increase surface charge negativity), which may improve colloidal stability. B^2: Slight increase in ZP with high stirring speed suggests minor effects on charge at extreme agitation. A model is considered significant when the F-value is 29.32. There is absolutely no way that an F-value this high could occur by chance (with a mere 0.01% likelihood). A p-value below 0.0500 indicates that the model terms are statistically significant.

The model highlights A^2, C^2, AB, BC, and A, B as significant factors. If the values are greater than 0.1000, the model terms will not be deemed relevant. When compared to the pure error, the Lack of Fit F-value does not reach statistical significance at a level of 0.45. A lack of fit F-value of this magnitude is most likely caused by noise, with a probability of 73.29%. There is less than 0.2 between the Adjusted R^2 of 0.9409 and the Predicted R^2 of 0.8660, which is within a reasonable range. Adequate precision is a device that measures the signal-to-noise ratio. A ratio greater than 4 is considered optimal.

A signal-to-noise ratio of 14.636 is considered satisfactory. The optimal ABC-NS formulation was established in Table 2 based on the factorial design research. The improved formula demonstrated an improved particle size of 164.53±2.15 nm, PDI of 0.135±0.01, EE of 89.63±0.64 & zeta potential of -24.36 ±3.26, in that order. The expected levels of A, B & C were used to generate three batches of ABC-N4S, which were then used to validate these values. Results from Y1, Y2, Y3 & Y4 (162.126, 0.135, 87.004 & -25.245) closely matched the expected values shown in Table 2. Isradipine nanoparticle preparation operational parameter predictions were as accurate as expected, proving the dependability of the optimised technique. Experimental investigations of *in vitro* release were performed on the chosen formulation.

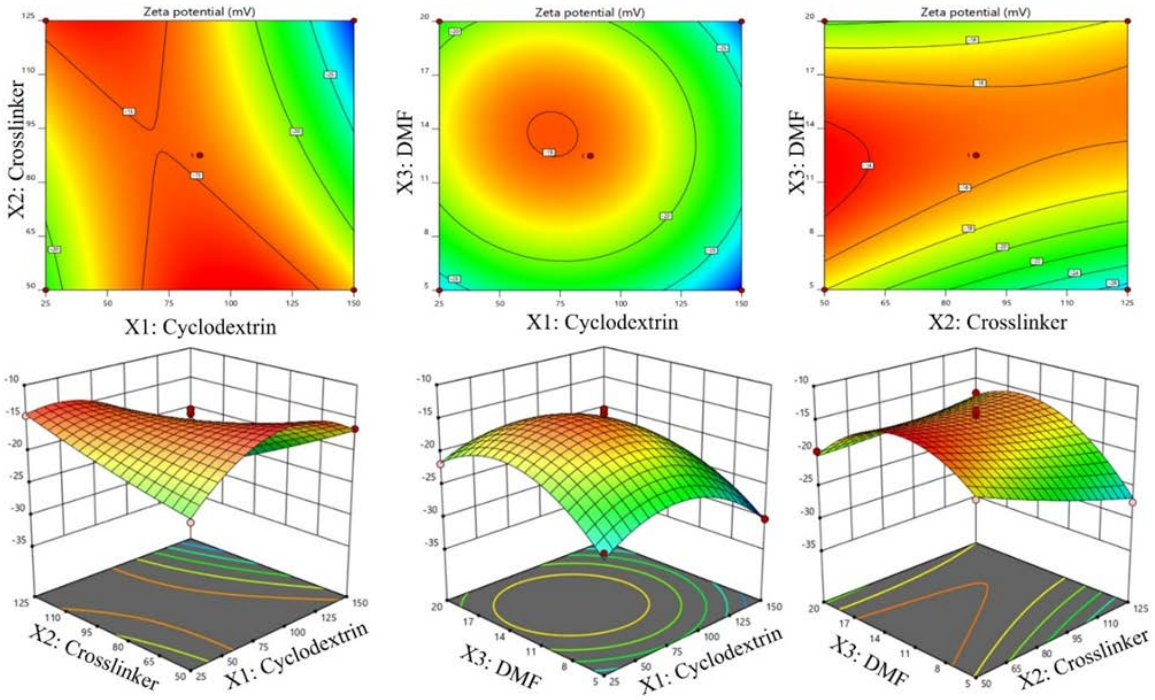

Figure 4: Contour response surface plot interaction between the independent variables on the ZP

Experimental validation of design space for formulation variables

Design of experiments (DOE) is an effective tool for minimising process variation, increasing product yield, and ensuring a consistent particle size distribution. One of the many tools employed was the Box-Behnken design, which allowed for the most efficient evaluation of the process parameters' primary, interaction, and quadratic effects on particle size, electrical

efficiency (EE), and practical yield. This structure allows you to study quadratic response surfaces and construct second-order polynomial models. Identical centre points and a set of coordinates located midway down each side of the three-dimensional cube make up the pattern. This kind of rotatable (or almost rotatable) system requires all three levels of every subsystem [35]. The response surface method, which is based on the Box-Behnken design, was used in seventeen separate investigations. Table 1 shows that various factor combinations produced varied results according to the experimental design.

The findings demonstrate a substantial dependence of the dependent variables on the independent factors, with a broad variance across 17 batches, as listed in Table 2. The formulation elements were examined using analysis of variance to determine their impact on the responses and their significance. Here are the findings of the study of variance (ANOVA) for PS, PDI, EE, and ZP, for responses 1, 2, 3, and 4, respectively, as shown in Table 3. Statistical analysis reveals a strong correlation between the three factors and the results. The optimal combinations of A and C were determined by optimising for Y1, Y2, Y3, and Y4. Y1, Y2, Y3, and Y4 are compared with their optimised levels and projected values. The following were derived from the analyses performed using Stat-Ease Design Expert software: regression equation, analysis of variance (ANOVA), and regression coefficients. The variables that were analysed are represented by the mathematical relationships that were established using multiple linear regression analysis [45].

Quantitative effects of varying polymer (A), (B), and (C) concentrations on vesicle size (Y1), PDI (Y2), EE (Y3), and zetapotential (Y4), together with their interactions, are shown in the following equations. The variables' effects on the Y1, Y2, and Y3 responses are associated with the A, B, and C coefficient values. Coefficients with higher-order terms indicate a quadratic connection, while those with multiple factor terms indicate an interaction term.

If the sign is positive, then the impact is synergistic, and if it is negative, then the effect is antagonistic. The data was fitted through a process of backward elimination to the quadratic model. In the ANOVA (Table 3), all of the polynomial equations were determined to be statistically significant ($P \leq 0.014$), according to the design expert software. According to the equation's output, A takes precedence over B and C. The primary and combined impacts of independent variables on particle size were better understood with the use of a counter and 3D response surface plots.

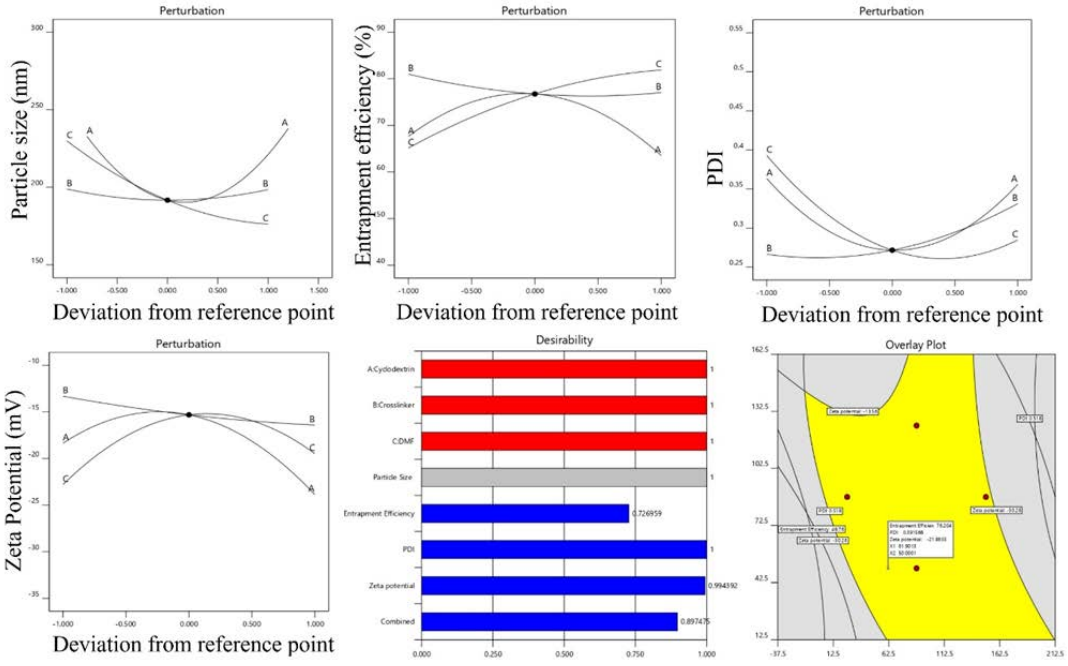

Figure 5: Perturbation plot showing the main effect of polymer concentration (A), cyclodextrin (B), and surfactant concentration (C) on Y1, Y2, and Y3, Optimized formulation of Desirability and overlay plot

The perturbation plot (Figure 5) illustrates how A, B, and C mostly impact the nanoparticle vesicle size (Y1). Here we can see that A is the most influential variable with respect to Y1, followed by B with a moderate influence, and finally C with a negligible one.

Table 3. ANOVA for the quadratic model.

Parameter	source	DF	Sum of squares	Mean of squares	F value	p-value
Y1	Model	9	20728.78	2303.20	64.05	< 0.0001
	Residual	7	251.70	35.96		
	Lack of fit	3	159.01	53.00	2.29	0.2205
	Pure error	4	92.69	23.17		
Y2	Model	9	1497.83	166.43	24.87	0.0002
	Residual	7	46.84	6.69		
	Lack of fit	3	12.15	4.05	0.4669	0.7212
	Pure error	4	34.69	8.67		
Y3	Model	9	0.1217	0.0135	54.53	< 0.0001
	Residual	7	0.0017	0.0002		
	Lack of fit	3	0.0014	0.0005	4.97	0.0778
	Pure error	4	0.0004	0.0001		
Y4	Model	9	539.99	60.00	29.32	< 0.0001
	Residual	7	14.32	2.05		
	Lack of fit	3	3.60	1.20	0.4470	0.7329
	Pure error	4	10.73	2.68		

Fourier-transform infrared spectroscopy (FTIR)

Figure 6 shows the FTIR spectra of the original drug and ABC. The peaks in the image are responsible for the few strong signals seen in the 400-4000 cm^{-1} wavelength range. The optimised ABC-NS spectrum demonstrated shifting of similar ABC peaks with intensity decrease in the drug's fingerprint area, according to the results. The fact that the drug was contained inside the polymer matrix is demonstrated by this. The presence of amide and amine groups was confirmed by the appearance of distinctive peaks in the pure Abemaciclib (drug) spectra, which were located around 3335 cm^{-1} (N–H stretching), 1650 cm^{-1} (C=O stretching of amide), and 1250–1300 cm^{-1} (C–N stretching). As is typical of its glycosidic connections, β-Cyclodextrin (B-CD) showed broad O–H stretching vibrations at 3400 cm^{-1} and C–O–C stretching near 1030–1150 cm^{-1}. The crosslinker showed CH_2/CH_3 bending in the region of 1400–1460 cm^{-1} and carbonyl (C=O) peaks around 1730 cm^{-1}. Significant broadening and displacement of the N–H peak (~3335 to ~3290 cm^{-1}) and C=O peak (~1650 to ~1625 cm^{-1}) were noted in the formulation of the ABC-loaded nanosponge.

These changes imply that Abemaciclib has formed hydrogen bonds and been encapsulated within the cyclodextrin nanosponge matrix, thereby validating molecular interactions between the medication and the polymer. The formulation's excellent encapsulation and molecular dispersion of the medication within the nanosponge network is indicated by the lack or attenuation of some drug-specific peaks (such as the strong C–N stretch at around 1250 cm^{-1}).

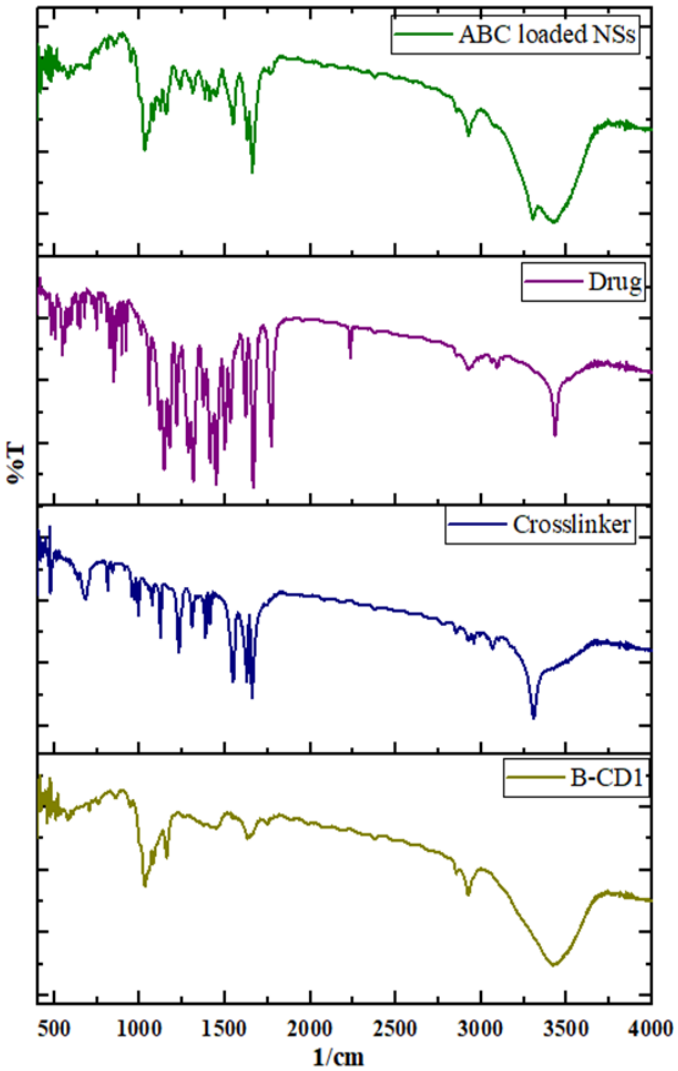

Figure 6: FTIR spectra of pure drug, cyclodextrin, crosslinker, and ABC-loaded nanosponges

Differential scanning calorimetry (DSC)

An indicator of whether or not a polymeric matrix has ensnared medicinal particles is to examine their thermal behaviour using DSC. The DSC thermograms of the optimised ABC-NS and pure ABC are shown in Figure 7. The physical state and thermal behaviour of Abemaciclib (ABC), β-cyclodextrin (B-CD), crosslinker, and the ABC-loaded nanosponges (NSs) were assessed by Differential Scanning Calorimetry (DSC). The crystalline nature of the pure substance was indicated by a prominent endothermic peak at about 180°C, which is also its melting point. Due to the loss of bound water and mild glass transition behaviour, B-CD showed a large endothermic peak in the 90–130°C range. The absence of a distinct peak confirmed its amorphous or semi-crystalline character. Around 190–200°C, the crosslinker displayed a clear and sharp endothermic peak, signifying a well-defined melting point and crystalline properties. The strong melting peak of pure Abemaciclib was absent from the thermogram of the ABC-loaded nanosponges. Instead, it showed wide transitions at about 180°C without any clear endothermic peak. The medication is distributed molecularly throughout the nanosponge matrix. The drug has been successfully encapsulated in an amorphous or solid solution form because no crystallinity has been retained. Strong interactions (such as hydrogen bonds) with cyclodextrin and crosslinker during nanoparticle formation are implied by the drug's melting peak disappearing.

There is an exothermic peak at 140.61 °C, two endothermic peaks at 129.53 and 184.32 °C, which were detected in thermogravimetric analysis of pure ABC, all of which were in agreement with the values stated in the US patent. In contrast, there is no discernible thermal peak of pure ABC in the optimised ABC-NS thermogram. The comparison showed that the EC polymer matrix entirely encased ABC in its spongy insides.

X-ray powder diffraction (XRD)

The XRD spectra of the optimised ABC-NS and the pure pharmaceutical ABC are shown in Figure 8. The crystallinity profiles of pure Abemaciclib (ABC), β-Cyclodextrin (B-CD), crosslinker, and the ABC-loaded nanosponge formulation were assessed using X-ray diffraction (XRD) analysis. Pure ABC's extremely crystalline nature was demonstrated by the strong and powerful diffraction peaks in the 2θ range of 10°–30° in its XRD pattern. Low aqueous solubility is linked to this high degree of crystallinity, which is a frequent feature of BCS Class IV medications like Abemaciclib. The crosslinker's crystalline state was confirmed by the clear, sharp peaks it displayed. A semi-crystalline or amorphous structure was suggested by the B-CD's collection of broad but distinct peaks. The XRD diffractogram of the pure drug, in line with other findings in the literature, showed several prominent angles: 6.00°, 6.80°, 12.00°, 15.40°, 18.60°, 21.00°, 26.2°, 38.10°, and 44.30° are the highest points. Optimised ABC-NS, on the other hand, had a lower peak density. This means that the medication was adequately confined inside the Nanosponge's polymer matrix. Optimised ABC-NS probably exhibited better amorphous behaviour due to the reduced crystallinity of the pure medicine, as demonstrated in Figure 8. By dispersing drug ABC into the EC polymer sponge, this clearly demonstrated a transition from a crystalline to an amorphous state. A polymeric sponge encases the medicine, preventing it from evaporating at the solid-air contact. On the other hand, the drug-loaded nanosponges' XRD pattern showed a broad halo devoid of noticeable peaks, indicating a total loss of crystalline order. This change implies that the medication is present in the nanosponge matrix in an amorphous or molecularly distributed state.

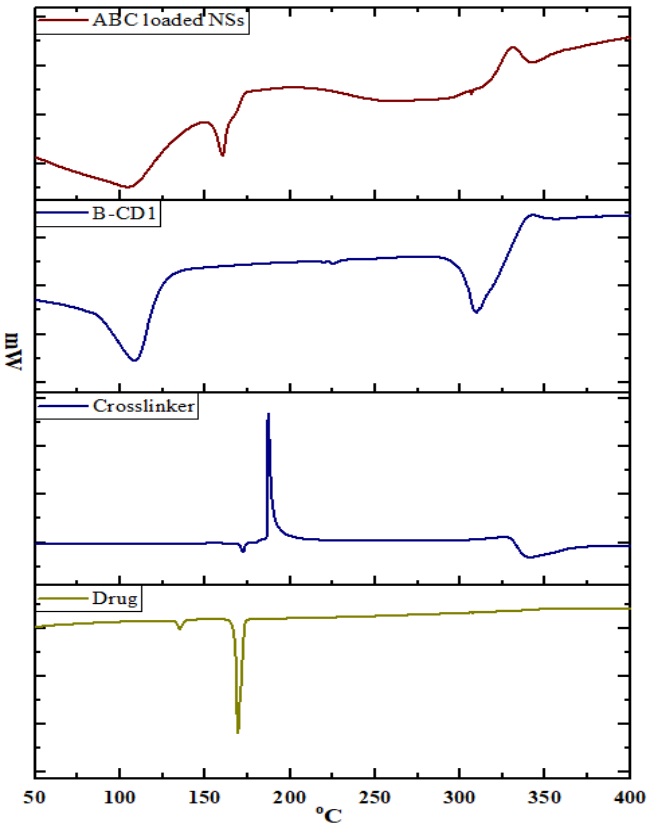

Figure 7: DSC thermograms of pure drug, cyclodextrin, crosslinker, and ABC-loaded nanosponges

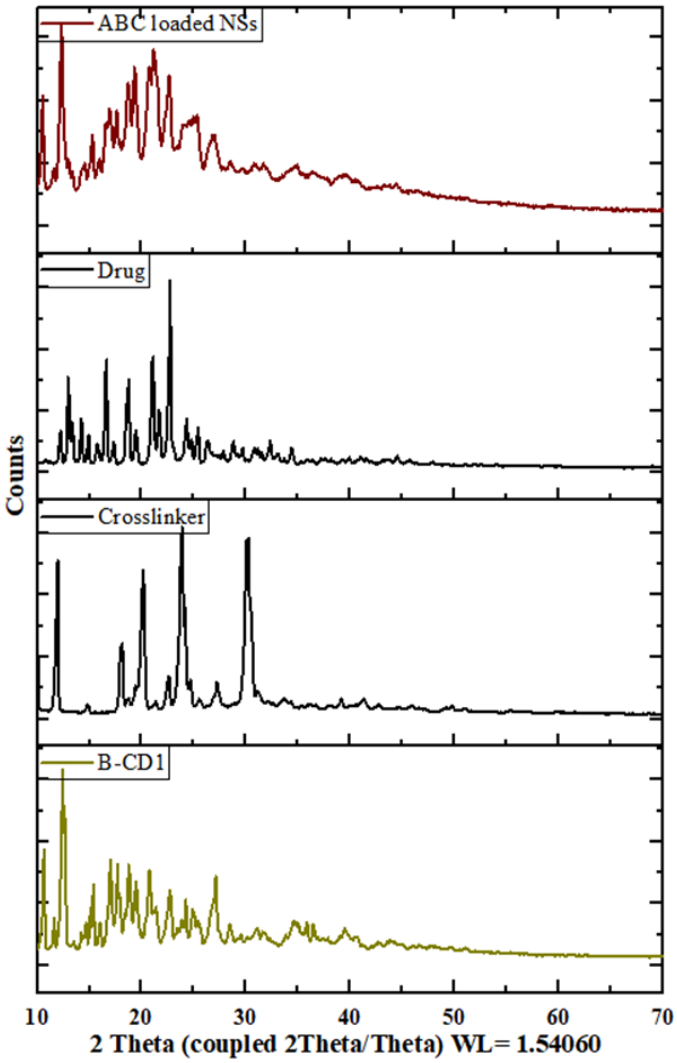

Figure 8: X-ray crystalography of pure drug, cyclodextrin, crosslinker, and ABC-loaded nanosponges

Scanning electron microscopy (SEM)

Scanning electron micrographs (SEMs) reveal crystallinity in both the pure drug (ABC) and the optimised ABC-NS (Figure 9), as well as the spherical form and smooth surface of the Nanosponge's porous structure, respectively. One possible explanation for the ABC-NS's porous structure is that DCM diffuses inward from the EC. The hydrophilicity of Kolliphore P-188 makes it a potential leachable material that might cling to the surface of the porous nanosponge during manufacturing.

***In-vitro* diffusion study**

The optimised nanosponge's drug release kinetics and mechanism were better understood thanks to this study. During formulation, a portion of Abemaciclib was adsorbed or weakly attached to the surface of the nanosponge particles, which is responsible for the initial burst release. Due to their partial entrapment inside the internal matrix, these surface-associated drug molecules are easily accessible for instantaneous diffusion into the surrounding liquid upon contact. Additionally, the porous structure of β-cyclodextrin-based nanosponges may facilitate the release of drugs close to or at the outer surface of the nanosponge network, allowing for initial solvent penetration.

The drug release occurred in a burst within four hours, as seen in Figure 10, and then continued steadily throughout the day. The optimised formulation and pure ABC suspension exhibited maximal drug releases of about 77.12% and 49.33%, respectively, at 24 hours. Moreover, the findings indicated that the drug's release characteristics from the NS were superior to those of the pure drug solution. Less water vapour can diffuse through the hydrophobic polymer structure, is likely responsible for the longer drug release from the optimised ABC-NS. When EC was present as a polymer, it greatly affected how ABC was released from the matrix. To determine the release mechanism, the optimised NS release data was subjected to many kinetic models.

There was a difference in the R^2 values of the zero-order, first-order, and Higuchi models: 0.7421 for zero-order, 0.7626 for first-order, and 0.8675 for the latter. The optimal release of ABC from the EC bilayer was likely caused by ABC diffusion across the optimised ABC-NS's porous and swellable matrix, since the Higuchi model had the highest R^2 value, making it the best fit for optimised ABC-NS. Additionally, a non-Fickian release mechanism was revealed by diffusion exponents in the Korsmeyer-Peppas model, which vary between 0.45 and 0.89.

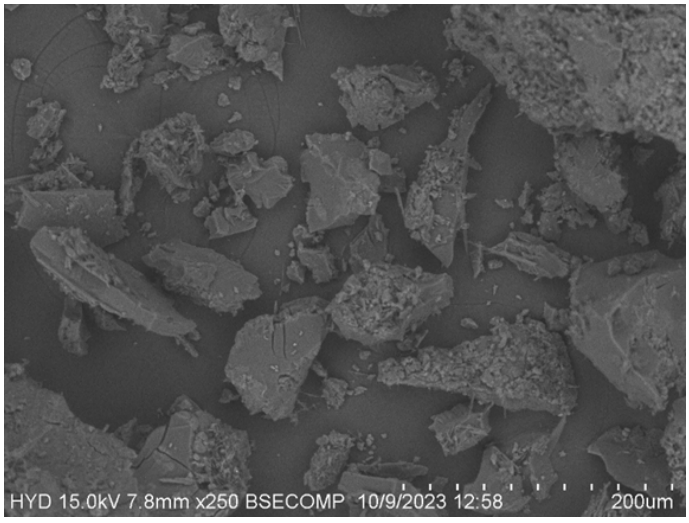

Figure 9: SEM image of optimized formulation

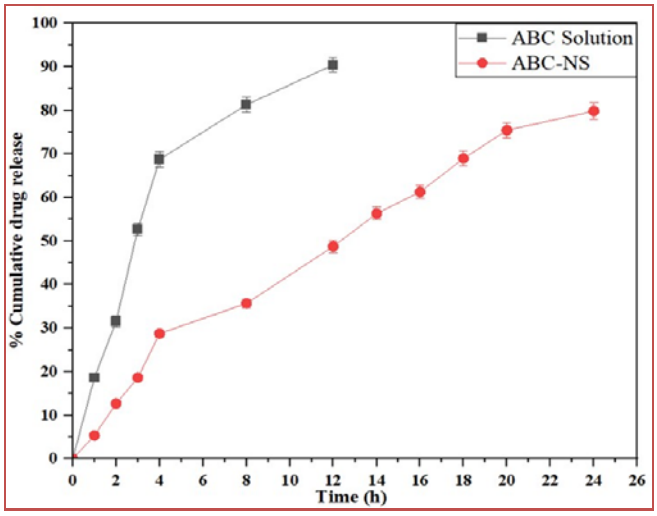

Figure 10: *In vitro* cumulative drug release profile of ABC Solution and ABC-NS over 24 h.

The ABC Solution shows a rapid release pattern, reaching >90% release within 10 hours, while the ABC-NS (nanostructured system) exhibits a sustained release profile, achieving approximately 80% release at 24 hours. Data are presented as mean ± SD (n = 3). The Higuchi model is based on Fickian diffusion and assumes drug release from a homogeneous matrix system, which aligns well with our nanosponge formulation. The porous architecture of β-cyclodextrin-based nanosponges facilitates diffusion-controlled drug release, which is the primary mechanism in our system, as supported by the sustained and linear release profile. Although the Korsmeyer–Peppas model is useful for identifying release mechanisms in polymeric systems, its empirical nature and reliance on the release exponent (n) make it less predictive for our matrix, where drug diffusion through interconnected pores is dominant.

Antioxidant activity

The enhanced ABC-NS was evaluated for its ability to scavenge DPPH radicals in a concentration range of 5-100 µg/mL, in comparison to both ABC and a standard (ascorbic acid). Figure 10 shows that optimised ABC-NS significantly reduced DPPH radicals via its scavenging action. The radical scavenging activity of optimised ABC-NS is 94.01% at 100 µg/mL. The antioxidant activity was shown to be much higher when ABC was combined with β-CD and DPC to create NSPs, as compared to pure ABC powder. The optimised ABC-NS of ABC shows comparable antioxidant activity to ascorbic acid at doses varying from 5 to 100 µg/mL. Our previously reported β-CD and diosmin combination was shown to have worse antioxidant activity compared to optimised ABC-NS. To determine whether there were any variations between standard ABC, we utilised Tukey's post hoc test and one-way ANOVA, formulation optimised ABC-NS, or ascorbic acid. Statistically significant (* $p < 0.05$), ascorbic acid and optimised ABC-NS demonstrated superior DPPH scavenging activity compared to plain ABC across all doses.

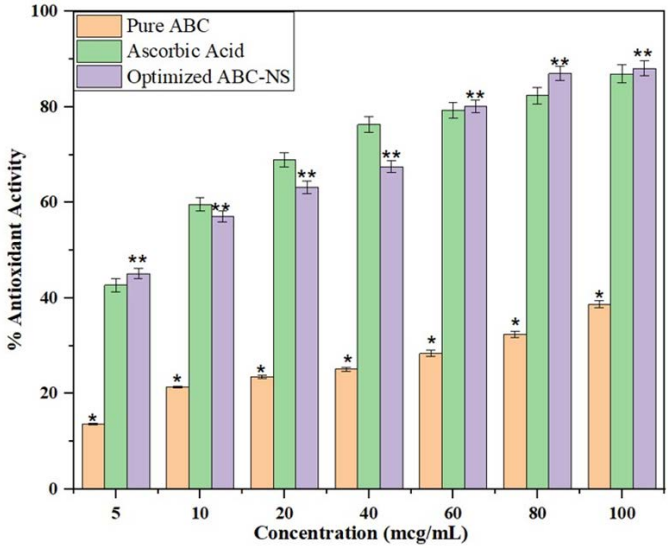

Figure 10: Antioxidant properties of optimised ABC-NS, ascorbic acid, and regular ABC compared. The results are given as an average with standard deviations, based on three measurements (mean ± SD, n = 3). * $p < 0.05$ indicates a significant difference between pure ABC and ascorbic acid, whereas ** $p < 0.05$ identifies a significant difference between optimised ABC-NS and pure ABC (at all doses) and the control. On the other hand, the optimised ABC-NS compared to ascorbic acid (at all doses) shows no significant difference (NS) when $p < 0.05$.

MTT assay

With respect to the MCF-7 and MDA-MB-231 cell lines, the MTT assay demonstrated that both the optimised Nanosponge and the pure medication exhibited a concentration-dependent decrease in cell viability (Figure 11). The absolute drug ABC had an IC50 value of 8.36 ± 0.31 µg/mL in the instance of MCF-7 cells, while the optimised ABC-NS had an IC50 value of 5.69 ± 0.27 µg/mL. Considering MDA-MB-231 separately, the readings were 19.67 ± 0.67 and 19.02 ± 0.35 µg/mL, respectively. At 6.25, 12.25.25, and 50 µg/mL, the cell viability of MCF-7 cells was considerably decreased by the optimised ABC-NS (45.36, 32.61, 25.94, and 22.13% at these concentrations), in comparison to pure drug ABC (54.13, 38.94,

31.02, and 27.84% at these same concentrations). In contrast, pure drug ABC resulted in a considerable decrease in MDA-MB-231 cells (71.24, 61.27, 45.32 and 23.15% at 6.25, 12.25. 25 and 50 µg/mL, respectively) compared to optimised ABC-NS (75.39, 62.15, 43.57 and 28.94% at 6.25, 12.25. 25 and 50 µg/mL, respectively). The MTT test results suggest that the optimised ABC-NS may have anticancer effects on breast cancer cell lines. This is most likely due to the fact that it released more medicine than the actual medication. Some study suggests that ABC-loaded NS could be a useful carrier for breast cancer therapy. The increased cytotoxicity is most likely caused by both enhanced cellular absorption and delayed intracellular drug release. The nanosponge system's porosity and nanoscale size facilitate endocytosis-mediated internalisation into cancer cells. After internalisation, the matrix permits gradual drug release, maintaining therapeutic intracellular concentrations over time. This prolonged exposure enhances drug–target interaction and results in higher cytotoxic effects than the pure drug, which may be removed or metabolised more quickly. The results are consistent with the dose- and time-dependent increase in cytotoxicity seen in the MTT experiment. The results confirmed that the nanosponge formulation exhibits significantly improved cytotoxicity, with statistically significant differences ($p < 0.05$) between ABC-NS and the free medication, especially at higher concentrations and longer exposure times.

However, we were unable to carry out these sophisticated cellular assays in the current investigation because of constraints in the equipment and resources that were available. To demonstrate the ABC-loaded nanosponges' potential for cytotoxicity, we instead used the tried-and-true MTT experiment.

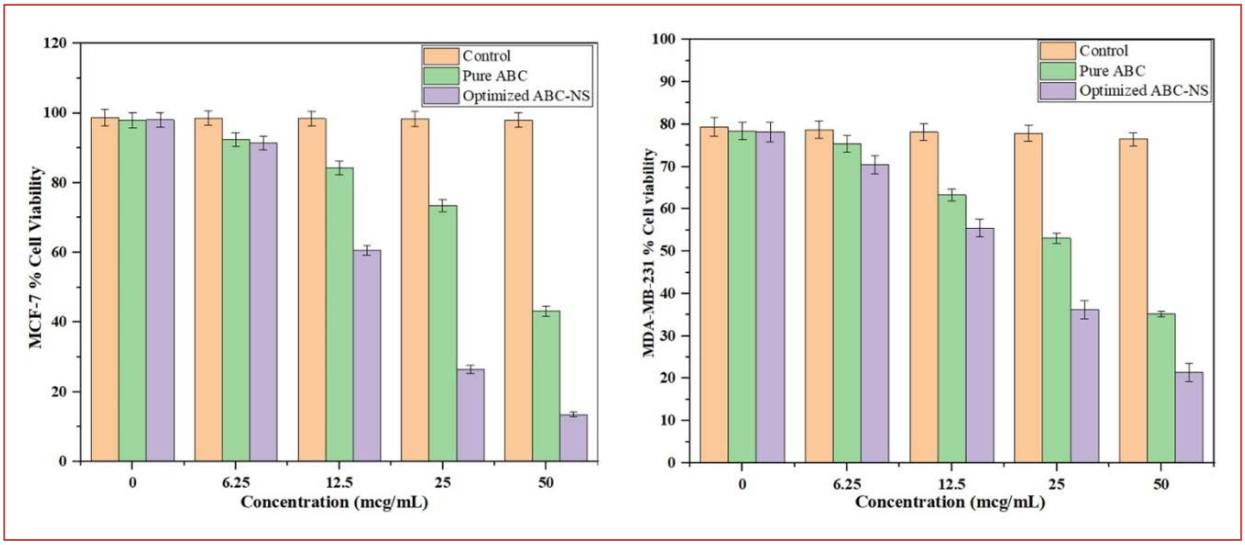

Figure 11: Comparative cytotoxicity analysis of Pure ABC and Optimized ABC-NS on MCF-7 and MDA-MB-231 cell lines. Cell viability (%) was assessed using an MTT assay after 24 hours of treatment with varying concentrations (6.25–50 µg/mL) of pure ABC and optimized ABC nanostructured system (ABC-NS). Results indicate a dose-dependent decrease in cell viability, with ABC-NS showing significantly enhanced cytotoxicity compared to pure ABC in both MCF-7 (left) and MDA-MB-231 (right) breast cancer cell lines. Data are presented as mean ± SD (n = 3).

The MTT test results on breast cancer cell lines suggest that the optimised ABC-NS may have anticancer effects. It most likely released more medicine than the pure medication, which explains this. According to certain research, ABC-loaded NS might be a useful carrier for breast cancer therapy. Improved cellular absorption and extended intracellular drug release are likely the causes of the increased cytotoxicity. Because of its porosity and nanoscale size, the nanosponge system improves endocytosis-mediated internalisation into cancer cells. The matrix maintains therapeutic intracellular concentrations over time by enabling gradual drug release following internalisation. More cytotoxic effects and improved drug–target interaction result from this prolonged exposure than from the pure drug, which may be removed or metabolised more quickly. According to the results, cytotoxicity increased in the MTT experiment in a dose- and time-dependent manner. At greater concentrations and longer exposure times, the results revealed statistically significant differences ($p < 0.05$) between ABC-NS and the free

medication, confirming the nanosponge formulation's markedly increased cytotoxicity. However, these sophisticated cellular assays could not be carried out in the current investigation due to constraints in the available resources and technology. Instead, we used the tried-and-true MTT assay to show that the ABC-loaded nanosponges have the ability to cause cytotoxicity.

CONCLUSION

The present study included the development and assessment of EC-based nanosponges loaded with ABC, focusing on their particle properties. The solvent emulsification-ultrasonication approach was deemed appropriate for the production of the nanostructures. By experimenting with different concentrations of the stabiliser Kolliphor P-188 and the sustained release polymer EC, the formulation was fine-tuned. The improved formulation met all requirements for its intended use in terms of PS, PDI, ZP, %EE, and %DL. Investigations utilising FTIR, DSC, XRD, and SEM demonstrated that the optimised ABC-NS was compatible with the polymer; the drug enclosed had an amorphous form and a spongy-smooth surface; and no significant chemical interactions were observed. After an initial burst release of the medication, a diffusion study of optimised ABC-NS showed a continuous release phase. The optimised ABC-NS demonstrated medication release of approximately 77.12% after 24 hours of release trials, whereas the pure ABC suspension showed drug release of around 49.33%. The optimised ABC-NS had a non-Fickian, asymmetrical release mechanism that adhered to the release kinetics concept put forward by Higuchi-Matrix. Finally, the improved ABC-NS demonstrated more sustained ABC release and demonstrated potential as an anticancer agent when tested against the MCF-7 and MDA-MB-231 breast cancer cell lines. As a result, the created material may prove to be a great vehicle for the anti-cancer chemical (ABC) in the treatment of breast cancer.

FINANCIAL ASSISTANCE

NIL

CONFLICT OF INTEREST

The authors declare no conflict of interest.

AUTHOR CONTRIBUTION

Conceptualization and draft preparation were carried out by Nirosha Bolledla. Vasudha Bakshi1 assisted in communicating, editing, and providing guidance. Both authors approved the final draft of the work.

REFERENCES

[1] Obeagu EI, Obeagu GU. Breast cancer: A review of risk factors and diagnosis. *Medicine*, **103(3),** e36905 (2024) http://dx.doi.org/10.1097/MD.0000000000036905

[2] Houghton SC, Hankinson SE. Cancer progress and priorities: breast cancer. *Cancer epidemiology, biomarkers and prevention*, **30(5),** 822-44 (2021) https://doi.org/10.1158/1055-9965.epi-20-1193

[3] Giaquinto AN, Sung H, Newman LA, Freedman RA, Smith RA, Star J, Jemal A, Siegel RL. Breast cancer statistics. *CA: a cancer journal for clinicians*, **74(6),** 477-95 (2024) https://doi.org/10.3322/caac.21863

[4] Liu J, He M, Wang Z, Li Q, Xu B. Current research status of metronomic chemotherapy in combination treatment of breast cancer. *Oncology research and treatment*, **45(11),** 681-92 (2022) https://doi.org/10.1159/000526481

[5] Aramini B, Masciale V, Grisendi G, Bertolini F, Maur M, Guaitoli G, Chrystel I, Morandi U, Stella F, Dominici M, Haider KH. Dissecting tumor growth: the role of cancer stem cells in drug resistance and recurrence. *Cancers*, **14(4),** 976 (2022) https://doi.org/10.3390/cancers14040976

[6] Nelson BE, Adashek JJ, Lin SH, Subbiah V. On target methods to induce abscopal phenomenon for Off-Target effects: From happenstance to happenings. *Cancer medicine*, **12(6),** 6451-65 (2023) https://doi.org/10.1002/cam4.5454

[7] Ding L, Cao J, Lin W, Chen H, Xiong X, Ao H, Yu M, Lin J, Cui Q. The roles of cyclin-dependent kinases in cell-cycle progression and therapeutic strategies in human breast cancer. *International journal of molecular sciences*, **21(6),** 1960 (2020) http://dx.doi.org/10.3390/ijms21061960

[8] Pellarin I, Dall'Acqua A, Favero A, Segatto I, Rossi V, Crestan N, Karimbayli J, Belletti B, Baldassarre G. Cyclin-dependent protein kinases and cell cycle regulation in biology and disease. *Signal transduction and targeted therapy*, **10(1),** 11 (2025) https://doi.org/10.1038/s41392-024-02080-z

[9] Tchakarska G, Sola B. The double dealing of cyclin D1. *Cell cycle*, **19(2),**163-78 (2020) https://doi.org/10.1080/15384101.2019.1706903

[10] Jeffreys SA, Becker TM, Khan S, Soon P, Neubauer H, de Souza P, Powter B. Prognostic and predictive value of CCND1/Cyclin D1 amplification in breast cancer with a focus on postmenopausal patients: a systematic review and meta-analysis. *Frontiers in endocrinology*, **13,** 895729 (2022) https://doi.org/10.3389/fendo.2022.895729

[11] Zhang M, Zhang L, Hei R, Li X, Cai H, Wu X, Zheng Q, Cai C. CDK inhibitors in cancer therapy, an overview of recent development. *American journal of cancer research*, **11(5),** 1913 (2021) https://pmc.ncbi.nlm.nih.gov/articles/PMC8167670/

[12] Mounika P, Gurupadayya B, Kumar HY, Namitha B. An overview of CDK enzyme inhibitors in cancer therapy. *Current*

cancer drug targets, **23(8),** 603-19 (2023) https://doi.org/10.2174/1568009623666230320144713

[13] Asnaashari S, Amjad E, Sokouti B. Synergistic effects of flavonoids and paclitaxel in cancer treatment: a systematic review. *Cancer cell international*, **23(1),** 211 (2023) https://doi.org/10.1186/s12935-023-03052-z

[14] Gerosa R, De Sanctis R, Jacobs F, Benvenuti C, Gaudio M, Saltalamacchia G, Torrisi R, Masci G, Miggiano C, Agustoni F, Pedrazzoli P. Cyclin-dependent kinase 2 (CDK2) inhibitors and others novel CDK inhibitors (CDKi) in breast cancer: clinical trials, current impact, and future directions. *Critical reviews in oncology/hematology*, **104324** (2024) https://doi.org/10.1016/j.apsb.2020.05.001

[15] Yuan K, Wang X, Dong H, Min W, Hao H, Yang P. Selective inhibition of CDK4/6: A safe and effective strategy for developing anticancer drugs. *Acta pharmaceutica sinica B*, **11(1),** 30-54 (2021) http://dx.doi.org/10.2174/0115734137288288240108073034.

[16] Goel S, Bergholz JS, Zhao JJ. Targeting CDK4 and CDK6 in cancer. *Nature reviews cancer*, **22(6),** 356-72 (2022) https://doi.org/10.1038/s41568-022-00456-3

[17] Ettl T, Schulz D, Bauer RJ. The renaissance of cyclin dependent kinase inhibitors. *Cancers*, **14(2),** 293 (2022) https://doi.org/10.3390/cancers14020293

[18] Fassl A, Geng Y, Sicinski P. CDK4 and CDK6 kinases: From basic science to cancer therapy. *Science*, **375(6577),** eabc1495 (2022) https://doi.org/10.1126/science.abc1495

[19] Piezzo M, Cocco S, Caputo R, Cianniello D, Gioia GD, Lauro VD, Fusco G, Martinelli C, Nuzzo F, Pensabene M, Laurentiis MD. Targeting cell cycle in breast cancer: CDK4/6 inhibitors. *International journal of molecular sciences*, **21(18),** 6479 (2020) https://doi.org/10.3390/ijms21186479

[20] Julve M, Clark JJ, Lythgoe MP. Advances in cyclin-dependent kinase inhibitors for the treatment of melanoma. *Expert opinion on pharmacotherapy*, **22(3),** 351-61 (2020) https://doi.org/10.1080/14656566.2020.1828348

[21] Saleh L, Wilson C, Holen I. CDK4/6 inhibitors in breast cancer–from *in vitro* models to clinical trials. *Acta oncologica*, **59(2)**, 219-32 (2022) https://doi.org/10.1080/0284186X.2019.1684559

[22] Chaurasia M, Singh R, Sur S, Flora SJ. A review of FDA approved drugs and their formulations for the treatment of breast cancer. *Frontiers in Pharmacology*, **14,** 1184472 (2023) https://doi.org/10.3389/fphar.2023.1184472

[23] Arora S, Narayan P, Osgood CL, Wedam S, Prowell TM, Gao JJ, Shah M, Krol D, Wahby S, Royce M, Ghosh S. US FDA drug approvals for breast cancer: a decade in review. *Clinical cancer research*, **28(6),** 1072-86 (2022) https://doi.org/10.1158/1078-0432.ccr-21-2600

[24] Leo CP, Leo C, Szucs TD. Breast cancer drug approvals by the US FDA from 1949 to 2018. *Nature reviews drug discovery*, **19(11),** (2020) https://doi.org/10.1038/d41573-019-00201-w

[25] Łukasik P, Baranowska-Bosiacka I, Kulczycka K, Gutowska I. Inhibitors of cyclin-dependent kinases: types and their mechanism of action. *International journal of molecular sciences*, **22(6)**, 2806 (2021) https://doi.org/10.3390/ijms22062806

[26] Mane PT, Wakure BS, Wakte PS. Cyclodextrin based nanosponges: a multidimensional drug delivery system and its biomedical applications. *Current drug delivery*, **18(10),** 1467-93 (2021) https://doi.org/10.2174/1567201818666210423091250

[27] Poulson BG, Alsulami QA, Sharfalddin A, El Agammy EF, Mouffouk F, Emwas AH, Jaremko L, Jaremko M. Cyclodextrins: Structural, chemical, and physical properties, and applications. *Polysaccharides*, **3(1),** 1-31 (2021) https://doi.org/10.3390/polysaccharides3010001

[28] Pyrak B, Rogacka-Pyrak K, Gubica T, Szeleszczuk Ł. Exploring cyclodextrin-based nanosponges as drug delivery systems: Understanding the physicochemical factors influencing drug loading and release kinetics. *International journal of molecular sciences*, **25(6),** 3527 (2024) https://doi.org/10.3390/ijms25063527

[29] Kapoor DU, Garg R, Saini PK, Gaur M, Prajapati BG. Nanomedicine breakthrough: Cyclodextrin-based nano sponges revolutionizing cancer treatment. *Nano-structures and nano-objects*, **40,** 101358 (2024) https://doi.org/10.1016/j.nanoso.2024.101358

[30] Wadhwa P, Vij M, Dand N. Wave-assisted techniques, a greener and quicker alternative to synthesis of cyclodextrin-based nanosponges: A review. *Recent patents on nanotechnology*, **18(2),** 207-19 (2024) https://doi.org/10.2174/1872210516666220928114103

[31] Al-Shdefat R, Hailat M, Alshogran OY, Abu Dayyih W, Gardouh A, Al Meanazel O. Ribociclib hybrid lipid–polymer nanoparticle preparation and characterization for cancer treatment. *Polymers*. **15(13),** 2844 (2023) https://doi.org/10.3390/polym15132844

[32] Shah, H. S., Zaib, S., Khan, I., Sliem, M. A., Alharbi, O., Al-Ghorbani, M., ... & Awan, S.. Preparation and investigation of a novel combination of Solanum nigrum-loaded, arabinoxylan-cross-linked β-cyclodextrin nanosponges for the treatment of cancer: in vitro, in vivo, and in silico evaluation. *Frontiers in Pharmacology*, **14,** 1325498 (2023) https://doi.org/10.3389/fphar.2023.1325498.

[33] Aboushanab AR, El-Moslemany RM, El-Kamel AH, Mehanna RA, Bakr BA, Ashour AA. Targeted fisetin-encapsulated β-cyclodextrin nanosponges for breast cancer. *Pharmaceutics*. **15(5)**, 1480 (2023) https://doi.org/10.3390/pharmaceutics15051480

[34] Mane PT, Wakure BS, Wakte PS. Enhancement in the therapeutic potential of lapatinib ditosylate against breast cancer by the use of β-cyclodextrin based ternary nanosponge system. *International journal of pharmaceutics*, **642,** 123210 (2023) https://doi.org/10.1016/j.ijpharm.2023.123210

[35] Rajalakshmi P, Peter DN, S JJ, Ananthi N. Structure-activity relationship of supramolecular compounds in drug delivery. *Mini-reviews in organic chemistry*, **18(7),** 961-89 (2021) http://dx.doi.org/10.2174/1570193X17999201123212536

[36] Tiwari K, Bhattacharya S. The ascension of nanosponges as a drug delivery carrier: preparation, characterization, and applications. Journal of Materials Science: *Materials in medicine*, **33(3),** 28 (2022) https://doi.org/10.1007/s10856-022-06652-9

[37] Avula PR, Chettupalli AK, Chauhan V, Jadi RK. Design, formulation, in-vitro and in-vivo pharmacokinetic evaluation of Nicardipine-nanostructured lipid carrier for transdermal drug delivery system. *Materials today proceedings*, (2023) https://doi.org/10.1016/j.matpr.2023.06.282

[38] Chettupalli AK, Ajmera S, Amarachinta PR, Manda RM, Jadi RK. Quality by Design approach for preparation, characterization, and statistical optimization of naproxen sodium-loaded ethosomes via transdermal route. *Current bioactive compounds*, **19(10),** 79-98 (2023) https://doi.org/10.2174/1573407219666230606142116

[39] Amarachinta PR, Sharma G, Samed N, Chettupalli AK, Alle M, Kim JC. Central composite design for the development of carvedilol-loaded transdermal ethosomal hydrogel for extended and enhanced anti-hypertensive effect. *Journal of nanobiotechnology*, **19,** 1–5 (2021) https://doi.org/10.1186/s12951-021-00833-4

[40] Sharaff CS, Renukuntla P, Peddapalli H, Kuchukuntla M, Bakshi V, Jadi RK. Formulation, development, and characterization of loratadine emulgel. *Journal of applied pharmaceutical research*, **12(2),** 42-50 (2024) https://doi.org/10.18231/j.joapr.2024.12.2.42.50

[41] Chettupalli AK, Rao PA, Kuchukuntla M, Bakshi V. Development and Optimization of Aripiprazole ODT by using box-Behnken Design. *Research journal of pharmacy and technology*, **13(12),** 6195–201 (2020) https://doi.org/10.5958/0974-360X.2020.01080.X

[42] Chettupalli AK, Unnisa A, Peddapalli H, Jadi RK, Anusha K, Amarachinta PR. Development and evaluation of empagliflozin-loaded solid lipid nanoparticles: Pharmacokinetics and pharmacodynamics for oral delivery. *Intelligent pharmacy*, (2025) https://doi.org/10.1016/j.ipha.2024.12.004

[43] Chettupalli AK, Ajmera S, Kuchukuntla M, Palanivel V, Katta S. Design Formulation of Nanospanlastic Novel Carriers as a Promising Approach to Enhanced Bioavailability in Intranasal Drug Delivery for Sinusitis: Statistical Optimization and In vitro and In vivo Characterization. *Current nanomedicine (Formerly: Recent patents on nanomedicine)*, **14(3),** 266-88 (2024) https://doi.org/10.2174/0124681873262019231105201433

[44] Prasad RR, Kumar JR, Vasudha BA, Kumar CA. Formulation development and evaluation of allopurinol solid dispersions by solvent evaporation technique. *International joural of applied pharmaceutics*, **10(4),** 168–71 (2018) http://dx.doi.org/10.22159/ijap.2018v10i4.25311

[45] Unnisa A, Chettupalli AK, Alazragi RS, Alelwani W, Bannunah AM, Barnawi J, Amarachinta PR, Jandrajupalli SB, Elamine BA, Mohamed OA, Hussain T. Nanostructured lipid carriers to enhance the bioavailability and solubility of ranolazine: Statistical optimization and pharmacological evaluations. *Pharmaceuticals*, **16(8),** 1151 (2023) https://doi.org/10.3390/ph16081151

[46] Sameina LH, Idamakantia S, Chettupalli AK, Velamala RR, Ezzat MO. Design of mesalamine loaded micro-particles: Preparation, in-vitro and in-vivo characterization. *Materials today: proceedings*, (2023) https://doi.org/10.1016/j.matpr.2023.07.063

[47] Chettupalli AK, Avula PR, Chauhan V. Improved Transdermal Delivery of Anti-hypertensive Drug Loaded Nanostructured Lipid Carriers: Statistical Design, Optimization, Depiction and Pharmacokinetic Assessment. *Current drug therapy*, **19(7),** 828–45 (2024) https://doi.org/10.2174/0115748855267831231113112445